JOURNAL OF PROPULSION AND POWER
Vol. 10, No. 1, Jan.–Feb. 1994

Dynamic Turbine Blade Temperature Measurements

William J. Becker,* Richard J. Roby,† and Walter F. O'Brien‡
Virginia Polytechnic Institute and State University, Blacksburg, Virginia 24061
and
Gerald K. Bensing§
Rosemount Aerospace Division, Eagan, Minnesota 55121

Turbine blade surface temperatures were studied during transient operation in a turbofan engine test rig. A single fiber radiation pyrometer was used to view the suction side of the blades from approximately 60% axial chord to the trailing edge at an average radial location of 70% blade height. A single ceramic-coated blade produced a once-per-revolution signal that allowed for the tracking of individual blades during the transients. The investigation concentrated on the light-off starting transient and the transients obtained during accelerating and decelerating between power settings. During starting and acceleration transients, the blade surface temperature gradient was observed to reverse. This phenomenon was most apparent during starting when the trailing edge was initially much hotter than the 60% chord location, resulting in large temperature gradients. In steady operation, the trailing-edge temperature was lower than the 60% chord location, and the gradients were less severe. During deceleration transients, the trailing edge cooled more rapidly than the 60% chord location. This resulted in larger temperature gradients than were seen in steady operation, but no profile inversion was observed. These temperature gradients and profile inversions represent a cycling of thermally induced stresses which may contribute to low-cycle fatigue damage. A simple one-dimensional heat transfer model is presented as a means of explaining the different heating rates observed during the transients.

Introduction

CONSIDERABLE improvements in turbine blade materials coupled with recent efforts in the development of air-cooled turbine blades have allowed higher turbine inlet gas temperatures. In the turbofan engine, higher turbine inlet temperatures result in improved thrust and specific fuel consumption as a result of increased thermal efficiency.[1] The desire to utilize this improved performance has led gas turbine manufacturers to increase turbine inlet temperatures. However, achieving the highest possible turbine inlet temperature requires accurate knowledge of the turbine blade temperatures for control and for prolonging engine life. The need for such knowledge has prompted much research in developing various techniques for measuring blade temperatures.

The tradeoff of these increased temperatures is the increased risk of experiencing a blade failure. Failure can be defined in many ways, but is most conveniently defined as any occurrence that requires removal of the blade from the engine. Under steady operation at elevated temperatures, problems arise in the form of blade creep and oxidation. The extent of damage resulting from both creep and oxidation is determined by the amount of time a blade is operated at a given temperature.

Another possible mode of blade failure is pitting or cracking due to low-cycle fatigue. For the Pratt and Whitney JT15D-1 engine used in this investigation, any observable cracks, or pits greater than 0.005-in. (0.127-mm) deep will require the blade to be repaired or replaced.[2] Majumdar[3] argues that low-cycle fatigue is related to transient temperature gradients and rotor speed. During transient operation, overshoots in both temperature and rotor speed can result in low-cycle fatigue damage. Halford[4] claims that most of the cyclic fatigue loading is due to severe thermal cycling associated with engine startup and shutdown. The large temperature gradients and high temperatures experienced during the start of the engine can lead to localized problems. The extent of the damage is dependent on the severity and duration of the transient.

Various methods of measuring blade temperatures exist, but the radiation pyrometer provides the fast response time needed to record transient data. Another measurement technique involves embedding thermocouples in the blade itself. However, difficulties arise in transmitting signals and in the inherent slow response time of thermocouples.

Benyon[5] points out that a major advantage of pyrometers is the inherent exponential response to target temperatures. This is especially beneficial for pyrometers used for engine control since the limiting high temperatures will result in a good signal-to-noise ratio. Increased digital signal processing speed has resulted in additional advantages which may be offered by pyrometers, including the ability to obtain temperature profiles at very high rotor speeds. This latter advantage involves the possibility of using a once-per-revolution signal from the pyrometer as an accurate real-time speed sensor.

Pyrometers, however, do have their disadvantages. Measurement errors are due mainly to spurious radiation and lens contamination.[6] Reflected radiation and transient interference from flames and glowing particles result in an additive or one-sided error which is always biased high. Conversely, errors due to lens contamination result in lower measured temperatures than actually exist. This latter problem is of major importance for engine control considerations due to the resulting fail-dangerous situation.

The present investigation utilized a single fiber radiation pyrometer with a small focus spot to measure transient temperatures on the surface of the first stage turbine blades of the engine test rig. Blade temperature profiles were recorded

Presented as Paper 89-2689 at the AIAA/ASME/SAE/ASEE 25th Joint Propulsion Conference, Monterey, CA, July 10–12, 1989; received Oct. 31, 1992; revision received June 16, 1993; accepted for publication July 2, 1993.

*Graduate Student, Mechanical Engineering; currently Engineer, Pratt and Whitney, Government Business Operations, West Palm Beach, FL 33402. Student Member AIAA.
†Adjunct Professor, Mechanical Engineering. Member AIAA.
‡Professor, Mechanical Engineering. Member AIAA.
§Senior Development Engineer, Temperature Group, 1256 Trapp Road.

throughout starting, acceleration, and deceleration transients, which allowed for comparison among the various transients.

Experimental Arrangement

The rig used for this research program was a modified Pratt and Whitney JT15D-1 turbofan, a small twin-spool turbofan engine that produces approximately 2000-lb thrust using a bypass ratio of about 3. The single-stage centrifugal compressor produces a maximum pressure ratio of approximately 10. The turbine consists of a single-stage, high-pressure turbine followed by a dual-stage, low-pressure turbine. All stages of the turbine are uncooled.

The low-pressure turbine stator support assembly (commonly referred to as the "wishbone" section) was modified in order to accommodate three research pyrometers. A schematic of the modified wishbone section showing a typical pyrometer penetration is presented in Fig. 1. The modifications consisted of installing sight tubes in the wishbone section to support and align the pyrometer probes, and purge lines to carry purge air to cleanse the pyrometer lens. Situated at an angle to the flow, the sight tube passes between the low-pressure turbine casing and the combustor liner. This close proximity to the combustor subjects the pyrometer to high temperatures. However, this problem is partially alleviated by the cooling effect provided by the purge air. The purge system has the capability of using shop air from a separate compressor, or using compressor bleed air from the engine itself. Thin static pressure tap lines were also installed in the penetration both upstream and downstream of the pyrometer to provide a means of measuring the pressure differential across the pyrometer. This allowed for direct calculation of the purge airflow rate.

The high-pressure turbine disk was also modified. A single blade was removed from the disk and the suction side of the blade was coated with a ceramic coating. The coating used was Rockide H, which characteristically has a lower emissivity than the nickel alloy blades. The coating technology[7] was developed by the Pratt and Whitney Government Engine Business, and the coating procedure was performed by them for this investigation. The synchronizing signal produced by this blade allowed for the identification of given blades as well as signal processing.

A pyrometer probe was used to monitor and channel radiation from the suction side of the blades onto a photovoltaic cell located in the photodetector. A 45-ft, single-strand fiber optic cable was used to transport the radiation to the electronics housing that contains an InGaAs photodetector and a preamp. A voltage output from the preamp is transmitted to the pyrometer processor box. This processor performs both amplification and signal processing on the signal, resulting in a voltage that is digitized by the high-speed data acquisition system. This digitized data is then written to disk on the IBM PC-AT. The main components of the pyrometer temperature measurement system are illustrated in Fig. 2.

The pyrometer uses a single color scheme which integrates radiant energy over the wavelength range of the detector. The fiber optics and the lens are rigidly housed in the tip of the probe, while purge air is forced along the outer circumference. The lens is recessed into the probe a few millimeters and the pyrometer is prevented from bending by the supports at the end and midlength of the probe. There is a single strand fiber optic connector at the top of the probe, which mates with a similar connector on the 45-ft-long fiber optic cable, which carries the radiant energy to the photodiode and the preamp. These connections are very sensitive to alignment and can produce a significant error, but this is of little consequence to profile observation. However, this can lead to significant error for absolute temperature determination.

The geometry of the pyrometer penetration requires the pyrometer to view the blade at an angle looking radially inward. The geometry of the blade itself is such that the trailing edge is closer to the lens than the 60% chord location. Because of this, the pyrometer does not trace a constant radius path across the blade. The pyrometer views the 60% chord location at about 61% blade height. The path traced is such that the radial location of the target spot on the blade increases to about 80% blade height at the trailing edge. Since the distance from the lens to blade surface is different at each axial location

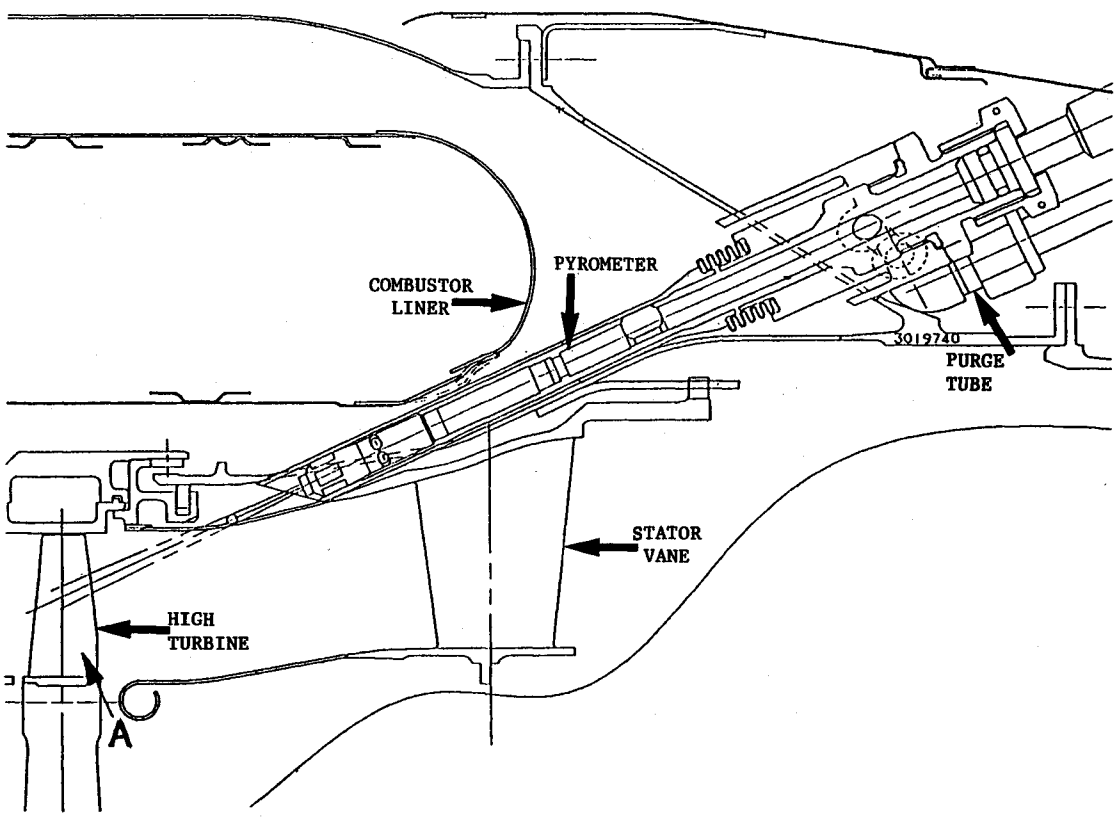

Fig. 1 Modified wishbone section showing pyrometer configuration.

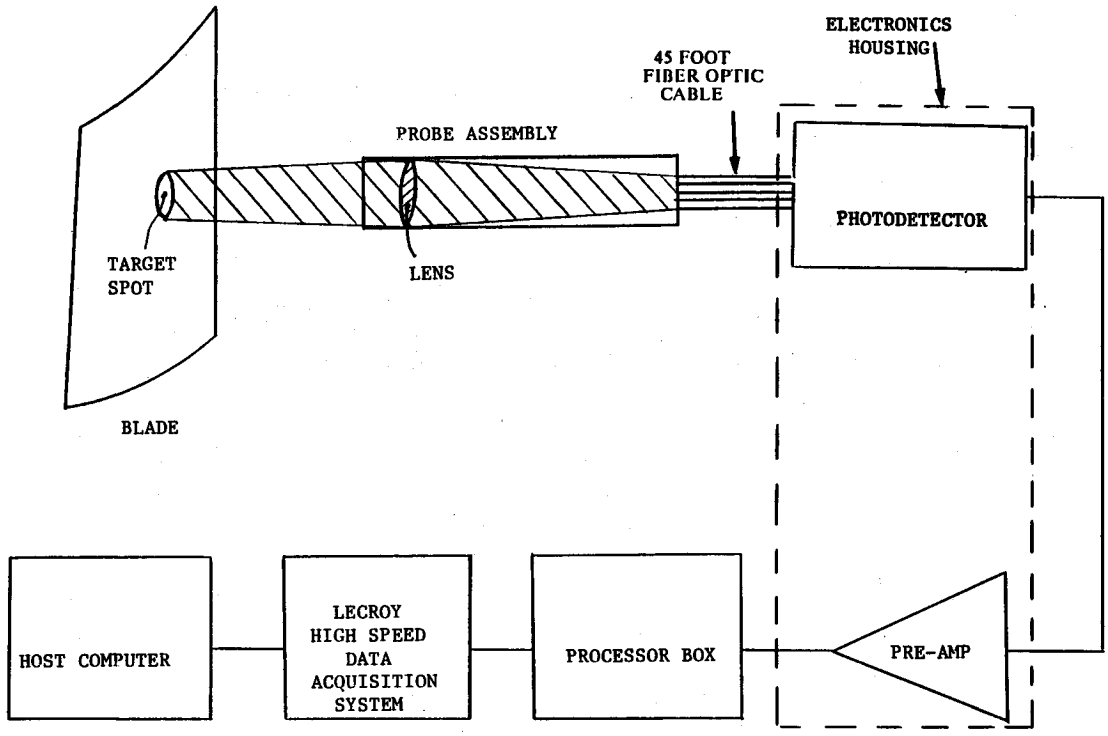

Fig. 2 Main components of pyrometer system.

on the blade, the distance from the focal plane to the blade is continually changing. This also causes a variation in target spot size as the pyrometer tracks across the blade. The result is a varying degree of "out of focus" of the pyrometer. Kirby[6] addresses this matter in detail and concludes that the error due to the pyrometer being out of focus is small relative to other possible errors and can usually be ignored.

One limitation of the pyrometer system used in this investigation was the lack of an easily applied calibration scheme. The effectiveness of the fiber optic couplings and the sooting of the lens are not constant from test-to-test, and thus, render any overall calibration inaccurate. However, data taken from previous test programs does provide a means of comparison. That is, previous results have yielded a curve relating average blade surface temperature to rotor speed. Data used to generate this curve were obtained using multispectrum pyrometry to obtain radiance data directly from the engine, from which the true blade temperatures were determined. For each start of this investigation, data were recorded at various speeds under steady operating conditions. Using the once-per-revolution signal, it was possible to relate average pyrometer output at these steady conditions to rotor speed. This information was used with the previous test results to relate pyrometer data obtained during this investigation to surface temperature at given rotor speeds. Knowing that pyrometer output increases exponentially with temperature, an exponential curve was fit to the data at these given rotor speeds. This curve was then used to relate all pyrometer output for a given test to temperatures. To ensure the best accuracy, a separate curve was generated for each test.

There is some error associated with the above calibration, but it is the best approximation of surface temperatures available. The accuracy of the temperatures depends on the accuracy of the previous test results used in the generation of the temperature vs rotor speed curve and the repeatability of the engine operation. The error associated with the absolute mean blade temperatures used in this calibration should be within ± 10 K.[8] However, the errors associated with the measurement of temperature differences will be less. This is because forming temperature differences eliminates the constant temperature offset produced by the calibration. The intent of this investigation was to focus on recording temperature profiles and trends occurring during transients; thus, only temperature differences were critical to this research.

Results

The suction sides of the turbine blades were studied at an average radial location of 70% blade height. Temperature profiles were obtained for steady operation and for several transient operating conditions including lightoff, acceleration, and deceleration. All sampling rates were selected such that approximately 30 or more data points per blade were recorded. The results of these investigations are presented in the following sections.

Steady-State Temperature Profiles

The coated blade has a surface treatment of Rockide H ceramic coating that is approximately 9-mm wide. However, the entire surface seen by the pyrometer is not covered by the coating. The pyrometer sees exposed blade surfaces at both the 60% chord and trailing-edge sides of the strip. Because of this, the coated blade produces pyrometer signals which are considerably different during steady operation and starting transients. The coated blade signal as it appears during steady operation is presented in Fig. 3. Since the emissivity of the coating is different from that of the blade material, the temperatures presented for the coated blade are not valid. However, this blade was used exclusively for identification purposes and no attempt was made to predict the effect of the coating on the temperature of that blade. Also shown in Fig. 3 are the blades immediately preceding and following the coated blade. These data were taken at a constant 85% N2 speed and sampled at a frequency of 1 MHz. This resulted in approximately 30 data points per blade. From these signals, it is seen that under steady conditions the trailing edge is the coolest part of the blade, while the 60% chord location is the hottest spot. This accounts for the initial increase in measured temperature level of the coated blade, followed by a sharp decrease as the coating is encountered.

Starting Transient

For each start recorded, 128 segments of data were taken each with a triggering period of 0.25 s. This amounted to a

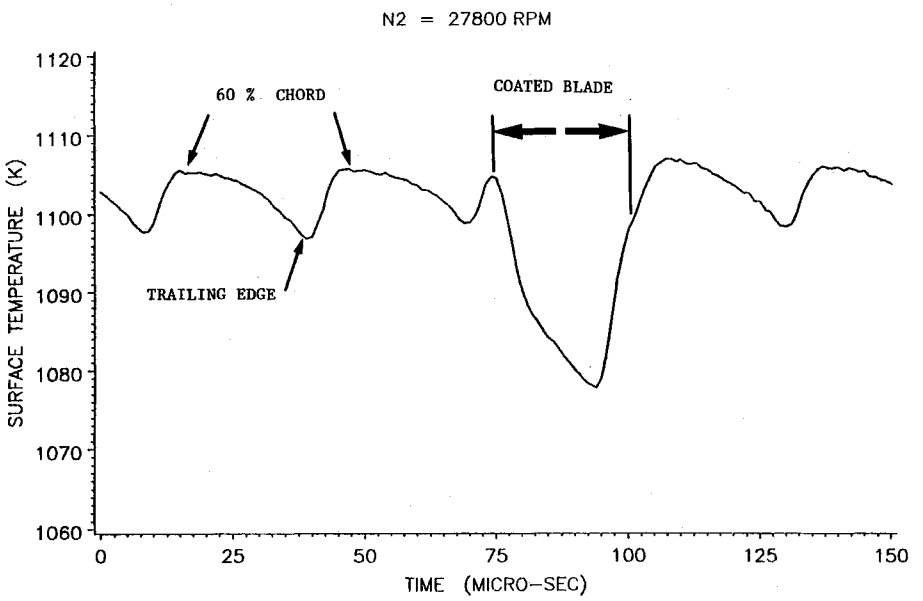

Fig. 3 Coated blade profile during steady operation.

total of about 32 s of the transient, which proved to be sufficient time to capture the entire transient. All of the starting transients were recorded in identical fashion. The results presented concentrate on data obtained during one typical start.

Figure 4 shows a sequence of chordwise temperature profiles for start number one at various times during the engine startup, while the entire transient temperature behavior of two points on the surface of a single blade is summarized in Fig. 5. The latter plot represents a temperature history of the 60% chord location as compared to that of the trailing edge. The data presented in all of the temperature histories shown in this section are taken from the blade immediately preceding the coated blade.

From Fig. 5, it can be seen that the trailing edge is heated considerably faster than the 60% chord location, and both temperatures overshoot the steady operation (idle) temperature. Results from previous test programs have revealed steady idle temperatures to be approximately 810 K. This rapid heating of the trailing edge leads to large temperature gradients early in the transient. After the peak temperatures of both locations have been reached, the trailing edge begins to be cooled at a faster rate than the 60% chord location. This eventually leads to an inversion of the temperature profile, represented graphically by the intersection of the two lines in Fig. 5. After this time the trailing edge remains the coolest part of the blade, and the blade temperature distribution eventually settles into a steady condition. This steady-state condition at idle has a very small peak-to-peak temperature variation on the order of 2–4 K.[8]

There are three distinct phases of each starting transient. Referring to Fig. 5, region I is the early part of the transient in which the trailing edge is hottest. Typical blade temperature profiles during this period are presented in Figs. 4a–4d. Characteristics of this phase are a hotter trailing edge and very large temperature gradients. The second distinct phase (region II) is that in which the blade surface temperature profile passes through a point of no slope. That is, there is no chordwise temperature gradient on the blade surface. A typical temperature profile from this part of the transient is presented in Fig. 4e. The last part of the transient (region III) is characterized by having a cooler trailing edge than 60% chord location. Typical temperature profiles from this portion of the transient are presented in Fig. 4f. These profiles closely represent those of steady operation, having much smaller temperature gradients than during the first part of the transient. Note also that the coated blade now has a small spike at the 60% chord location, which is characteristic of steady operation.

Temperature histories similar to those presented in Fig. 5 were obtained for the other starting transients recorded. All transients were recorded on different occasions, but under similar conditions. The trends of each start are the same, but the settling time and time of profile inversion vary. This is evidence that the engine operator, starter operation, and other factors play a role in the temperature transients, and therefore, the severity of the thermal gradients for a given start.

Acceleration Transient

Acceleration transients were recorded as the engine was accelerated between power settings by way of a quick throttle change. These transients differ from starts in that acceleration transients start and end with steady profiles and are typically much less severe. Figure 6 shows chordwise temperature profiles at various times during the transient. Figure 7 shows a temperature history of both the 60% location and the trailing edge of the blade immediately preceding the coated blade. The transient was from 84% N2 to 88% N2.

From Fig. 7, it can be seen that even during this small range acceleration, two distinct temperature profile inversions were experienced. The acceleration transient also had three distinct regions, however, these regions were quite different from those depicted during the starting transient. The first part of the transient, denoted region A, is characterized as being similar to steady operation. A typical temperature profile during this period is presented in Fig. 6a, representing the transition from steady operation into a transient operating condition. It can be seen that the temperature profile is fairly flat over a good portion of the blade and makes a fairly sharp drop near the trailing edge. This results in a large gradient at the trailing edge, but not a very large temperature difference. Because of this small temperature difference, not much time is required for the trailing-edge temperature to exceed that of the 60% chord location when higher temperature gases are present during acceleration.

The period after this first inversion is the second distinct region in the transient, denoted as region B. A typical temperature profile from this period is presented in Fig. 6c. It should be noted that although the trailing edge is hotter than the 60% location, neither of the two locations are the hot spot of the blade. This occurs somewhere near the 90% chord location, creating an almost parabolic temperature profile. Toward the end of this period of the transient, the profiles began trending toward those for steady operation. Once again,

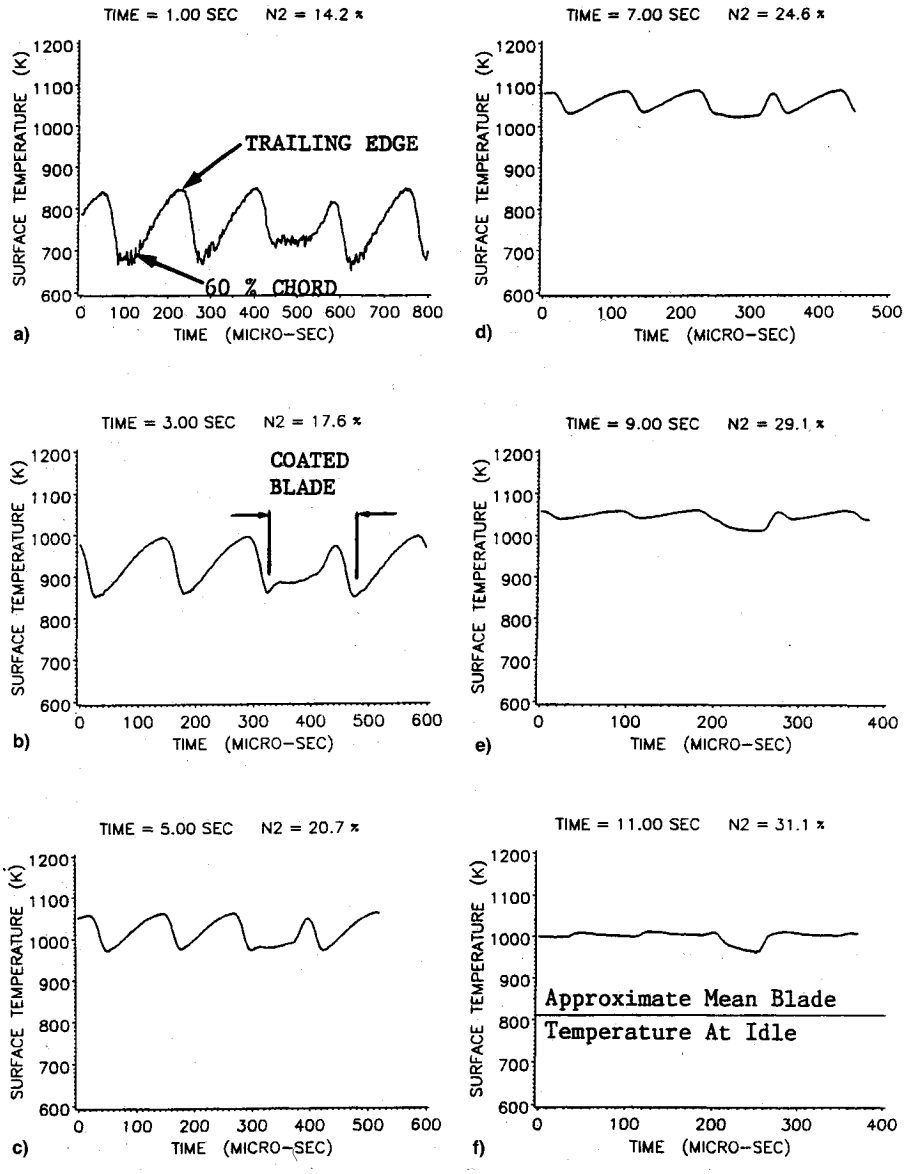

Fig. 4 Chordwise temperature profiles during starting transient no. 1.

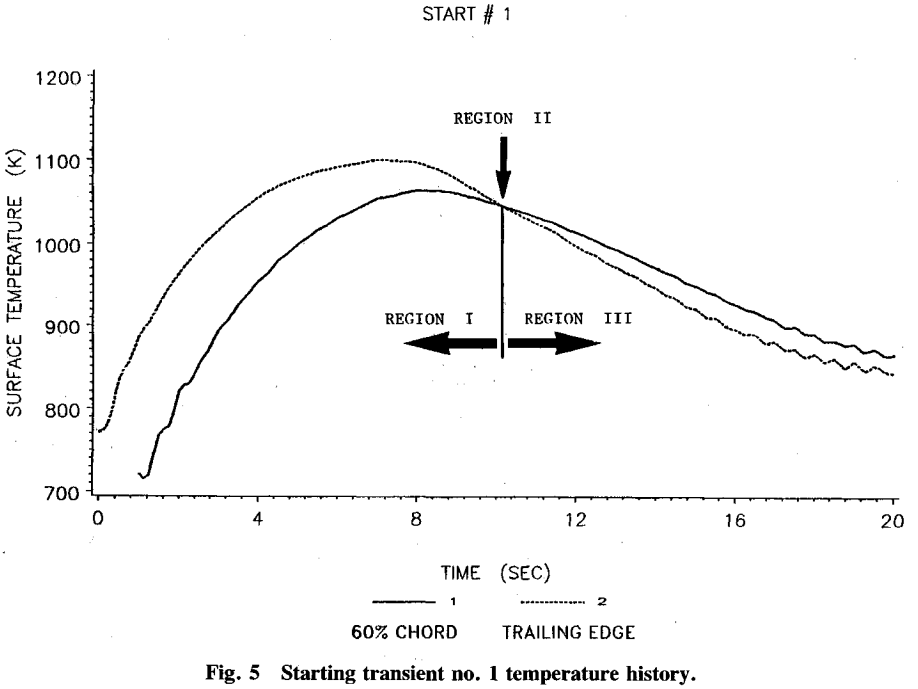

Fig. 5 Starting transient no. 1 temperature history.

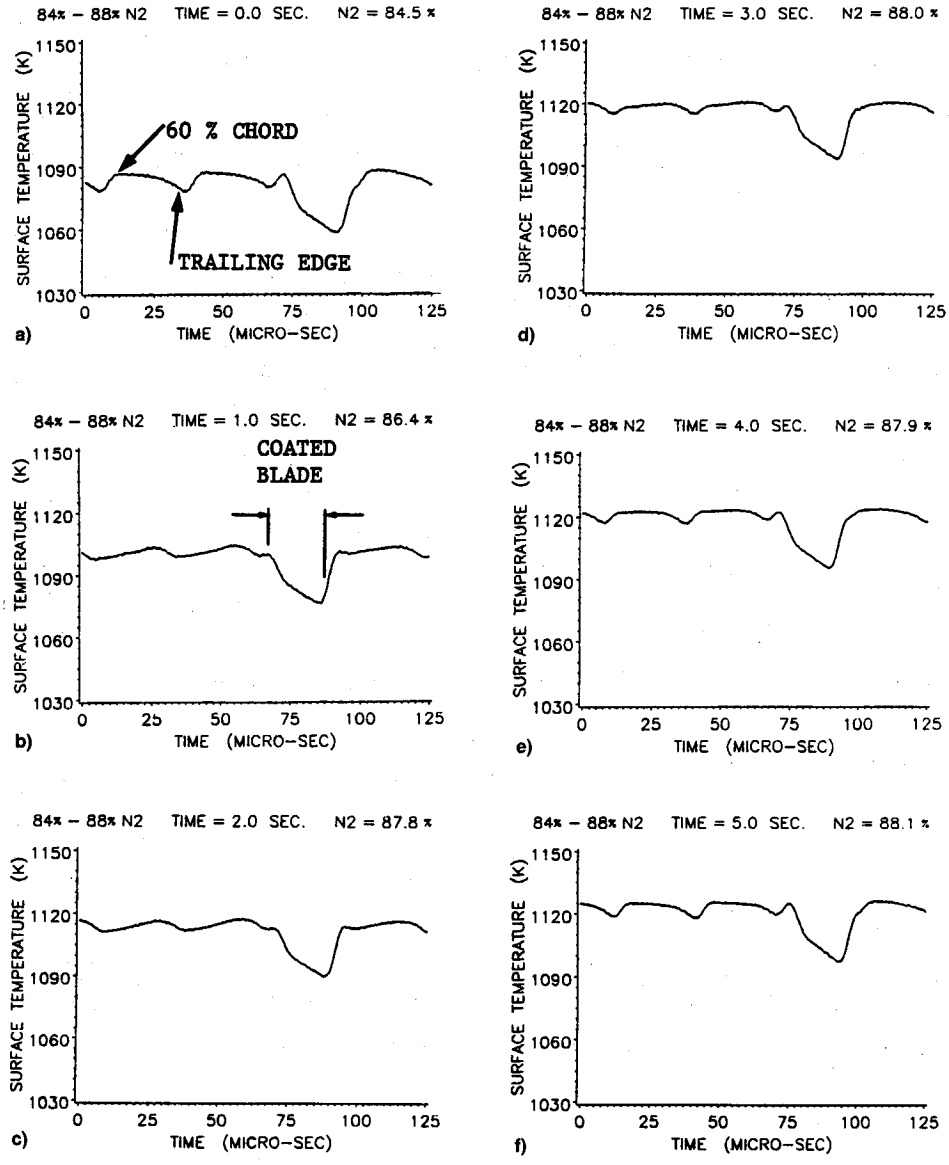

Fig. 6 Chordwise temperature profiles during acceleration.

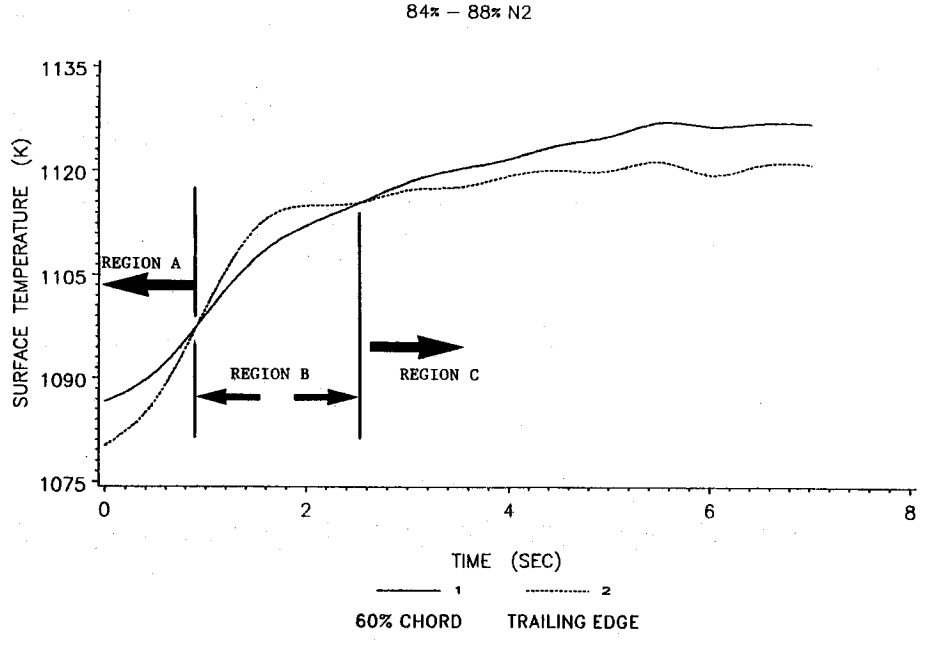

Fig. 7 Acceleration transient temperature history.

a temperature gradient inversion was experienced and the trailing edge became the coolest spot of the blade.

This second inversion marks the start of the third distinct region of the transient. This period, region C in Fig. 7, is characterized as having temperature profiles similar to those for the final steady operating conditions. A typical temperature profile during this period can be seen in Fig. 6f. This plot reveals a slightly parabolic temperature profile as seen in the previous region. However, distinct characteristics of steady operation are evident. These include a cooler trailing edge as well as a coated blade profile that resembles that of steady operation as previously discussed. The previous 3 plots along with 12 others were used to develop the data used to generate the temperature history presented in Fig. 7.

Deceleration Transients

Several deceleration transients between power settings were recorded. The decelerations were generated by a quick throttle change between power settings. A sequence of chordwise temperature profiles of one deceleration is presented in Fig. 8. A temperature history of this deceleration transient is presented in Fig. 9. Once again, this plot was developed using data from the blade immediately preceding the coated blade. The transient was a deceleration from approximately 85% N2 to 75% N2.

The temperature history reveals characteristics considerably different from those of the starting and acceleration transients. The major difference is that no temperature inversion is experienced. During the initial steady operation, the trailing edge has the lowest surface temperature of the viewable portion of the blade. As the gas temperature is decreased, the trailing edge is cooled at a faster rate than the 60% chord location, which initially causes large temperature gradients. However, the 60% chord location is quickly cooled and the surface temperatures trend toward those for steady operation.

Discussion of Results

Analytical Model

Once the starting transient results were analyzed, a simplified model was developed in an attempt to analytically reproduce these results. It should be stated at the onset that the model presented is offered as only one possible explanation of the phenomena observed. The blade geometry is simplified and assumptions are made. For this reason, it is not intended to predict exact temperatures or temperature profiles, but merely to show trends of the predicted transient for comparison purposes.

Since the blade is much longer than it is thick in the region of interest, conduction in the axial direction is ignored in the model to be presented. Only conduction from the centerline

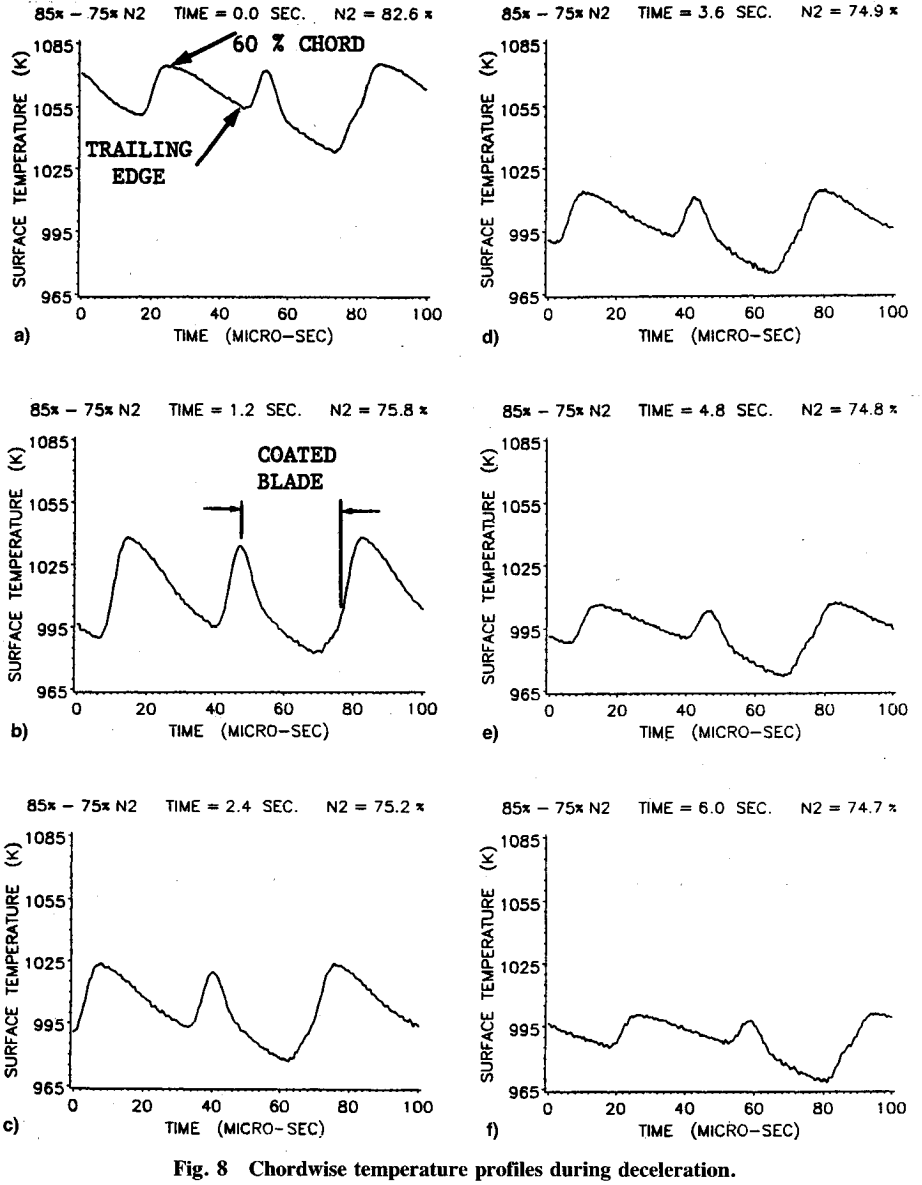

Fig. 8 Chordwise temperature profiles during deceleration.

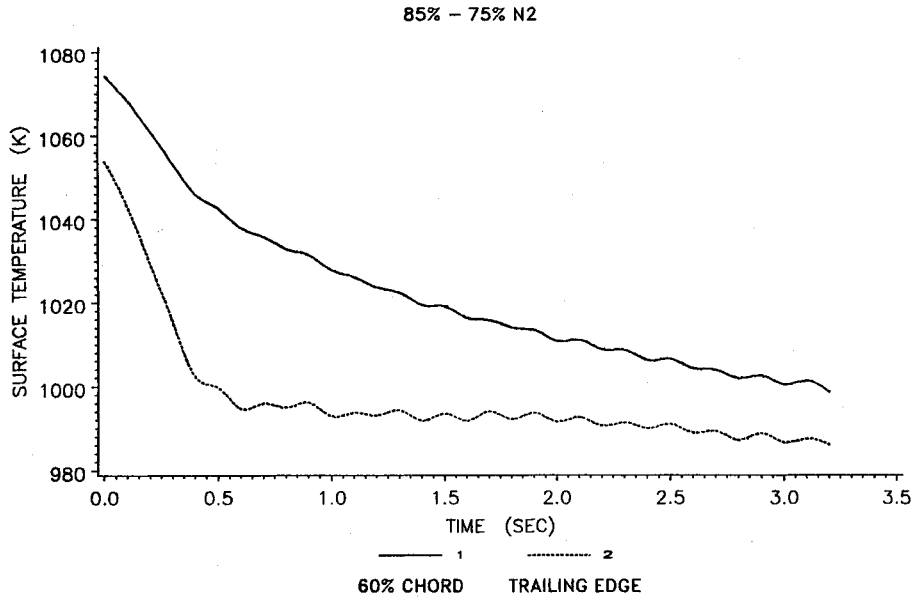

Fig. 9 Deceleration transient temperature history.

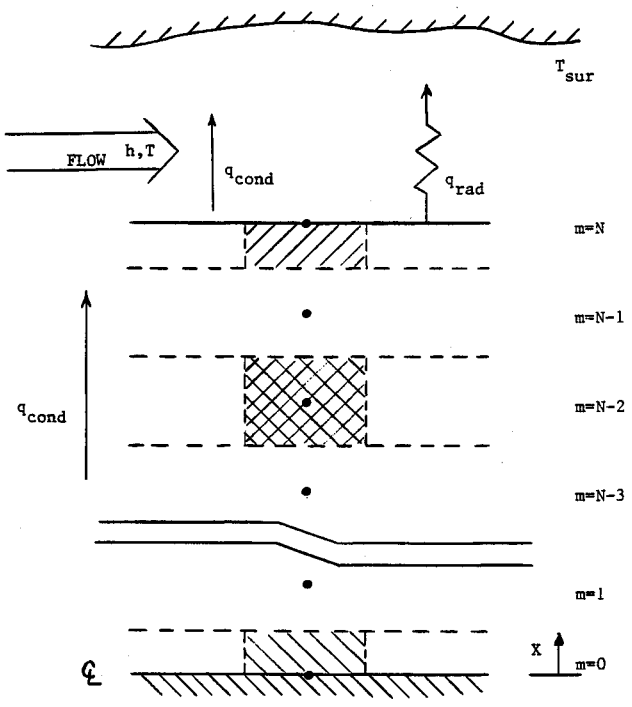

Fig. 10 Schematic of turbine blade heat transfer model.

out to the exposed surface is considered. Therefore, the geometry of the blade is reduced to simply the thickness of the blade at a given axial location. A symmetrical boundary condition is imposed on the centerline of the blade. In practice, this will not occur exactly at the centerline, but is a reasonable assumption given the intent of the model. The blade surface is subjected to convection from the gas flow as well as radiation to the surroundings. Blade geometry is such that the 60% suction side chord location radiates mainly to the pressure side of the neighboring blade. However, the trailing edge radiates to surfaces downstream of the high-pressure turbine. For this reason, the surrounding temperature seen by the trailing edge was taken to be 75% of that seen by the 60% chord location. This value was used because the temperature of the gas entering the low-pressure turbine is approximately 75% of the gas temperature entering the high-pressure turbine.[2] A schematic showing the model applied to a turbine blade is shown in Fig. 10.

A time history of the turbine inlet temperature was also needed. Knowing the trends of the ITT and the related maximum gas temperature, a reasonable profile was assumed as presented in Fig. 11. Since the gas temperature is not known exactly, no accuracy would be gained by varying the film coefficient with temperature. Because of this, a film coefficient was assumed and was held constant throughout the transient. An average thermal conductivity of the blade was used and considered constant also.

A finite difference model employing the above conditions was solved numerically. As with the starting transients obtained experimentally, only the 60% chord location and the trailing-edge temperature histories are presented. Various cases were run to check the effect of varying some of the parameters that were assumed constant. As expected, all cases exhibited the same trends, but the temperatures and lag times differed somewhat. The results of a typical case are shown in Fig. 12. Values for the film coefficient and the thermal conductivity used in this case were 3000 W/m^2 and 12 W/mK, respectively. The thermal conductivity value is the average value for the Inconel 100 blades over the expected temperature range. The plot shows the same trends as seen in the experimental results of the starting transients. The small temperature difference occurring as the transient approaches steady state is evidence that the effects of radiation are small. Though the effect will be somewhat greater during the transient than at steady state, this supports the conclusion that radiation is not the dominant mode of heat transfer during the transient. The effects of radiation should be most evident at steady operation as the blade approaches the freestream temperature.

Temperature Gradients

The analytical model presented has indicated that the transient temperature profiles are dominated mainly by convection to the blade and the thermal capacity of the blade. The more massive 60% chord location increases temperature at a slower rate than the trailing edge when subjected to the same gas temperature. The overshoot in turbine gas inlet temperature causes high temperatures at the trailing edge, resulting in large gradients. This overshoot in temperature is related to the inefficient operation of the compressor during the start phase, and the slow response time of the fuel control system. As the gas temperature is cooled to its steady value, the trailing edge cools at a faster rate than does the 60% chord location. This "reluctance" of the 60% chord location to release its stored energy results in an eventual temperature profile inversion. As the transient ends and steady operation

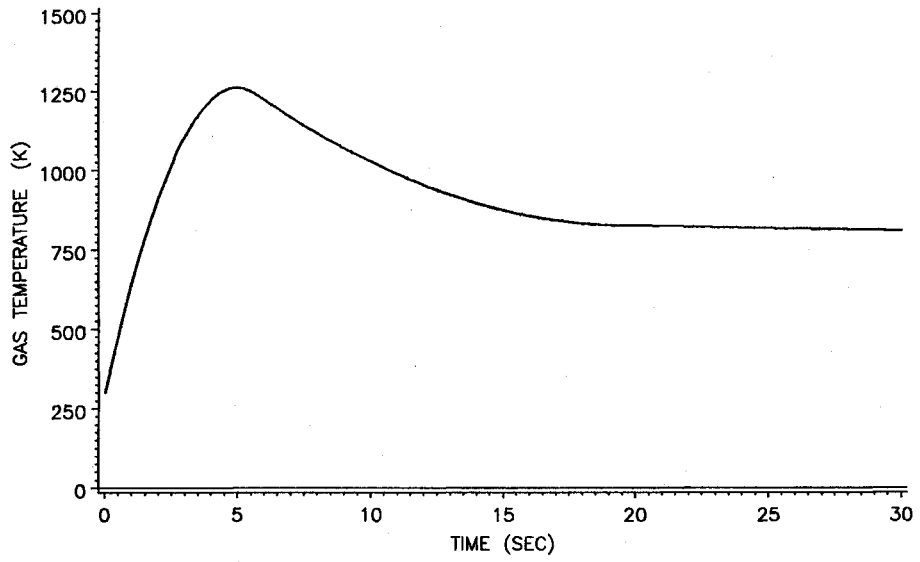

Fig. 11 Assumed turbine inlet gas temperature history (assumed for finite difference solution).

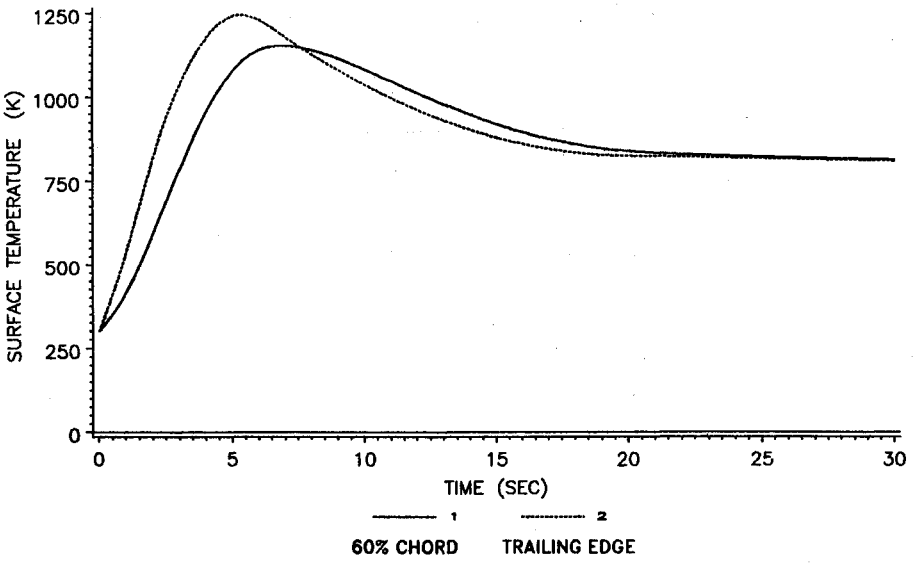

Fig. 12 Approximate finite difference solution of starting transient temperature history.

occurs, the effects of the thermal mass become small. The effects of the radiation are likely at least partly responsible for the lower measured surface temperature of the trailing edge of the blade.

Each of the transients presented were seen to cause an increase in surface temperature gradients during the transient, followed by a decrease in the gradient as the engine approached steady operation. This represents a cycle in the thermally induced stresses exerted on the blade. This thermal cycling results in low-cycle fatigue effects that have been observed to add to the effects of creep strain. Since the low-cycle thermal fatigue effects are related to temperature gradients during transients, accurate knowledge of transient temperature distributions is essential to determine effects of the transient on engine life.

The results indicate that starting transients cause the most severe gradients being on the order of 15.5 K/mm with very large gradients near the trailing edge of the blade. The gradients experienced during the deceleration transient were also large being on the order of 5.5 K/mm. These large gradients would likely result in large thermally induced stress on the turbine blade. The least severe test in terms of temperature gradients was the acceleration transient. However, the acceleration presented was fairly "gentle," and thus, the gradients should not be severe. In contrast, wide range accelerations might produce more severe temperature gradients.

Since fatigue effects combine with those of creep strain, accurate knowledge of transient temperature distributions may lead to an improved prediction of engine life for a given engine mission. It is most convenient to calculate engine life and maintenance intervals in hours of operation. Therefore, it is desirable to relate the fatigue effects to equivalent operating hours under steady conditions that would result in similar damage due to creep. The ability of the pyrometer to detect temperature gradients under transient conditions represents a technology which can be used to more accurately analyze the factors and effects of thermally induced low-cycle fatigue on engine life.

Conclusions

The thermal dynamics of the suction sides of the first stage turbine blades of a JT15D-1 research gas turbine under transient conditions were investigated. Using a single strand InGaAs radiation pyrometer, the blades were viewed from approximately 60% chord to the trailing edge. Included in the study were starting, acceleration, and deceleration transients.

The starting transients were found to be the most severe in terms of both peak temperature and temperature gradients. The experiments revealed that a reversal in the chordwise temperature gradient was occurring during the starting transient. Initially, the trailing edge was heated more quickly than was the more massive 60% chord location. This resulted in high temperatures at the trailing edge as well as large gradients. As the turbine inlet temperature and rotor speed approached their steady-state value, the trailing edge became cooler than the 60% chord location. The observed transient temperature changes appeared to be the result of thermal response lag of the blade material, based on the results of the simple analytical model.

The gradients experienced during the deceleration transients were less severe than those for the start, and no temperature gradient inversions were observed. During acceleration transients, the gradients became only slightly larger than at steady operation, but two temperature profile inversions were observed.

It has been argued that both overshoots in temperature and large temperature gradients are contributing factors to low-cycle fatigue. The results presented show that large temperature gradients are observed during the starting transients which would be associated with the most severe thermally induced stresses. Other transients would contribute to the damage, but were observed to be less severe in this investigation. The demonstrated ability of the pyrometer to record transient temperature distributions appears to be a valuable addition to low-cycle fatigue analysis and study.

Acknowledgments

The authors would like to thank Rosemount Aerospace Division for their financial support of the work reported above. In addition, the authors would like to thank Pratt and Whitney for their support in modifying the engine used in these studies.

References

[1]Kerrebrock, J. L., *Aircraft Engines and Gas Turbines*, MIT Press, Cambridge, MA, 1984, pp. 43–45.

[2]*Maintenance Manual Turbofan Engine Models JT15D-1, -1A, -1B, -4, -4B, -4D*, Manual Part 3017542, Pratt and Whitney Canada, Longueuil, Quebec, Canada, 1984.

[3]Majumdar, S., "Low-Cycle Fatigue and Creep Analysis of Gas Turbine Components," *Journal of Aircraft*, Vol. 12, No. 4, 1975, p. 381–389.

[4]Halford, G. R., "High-Temperature Fatigue in Metals—A Brief Overview of Life Prediction Methods Developed at The Lewis Research Center of NASA," SAMPE Quarterly, Vol. 14, No. 3, 1983, pp. 17–23.

[5]Benyon, T. G. R., "Turbine Pyrometry—An Equipment Manufacturer's View," American Society of Mechanical Engineers Paper 81-GT-136, May 1981, pp. 1–5.

[6]Kirby, P. J., "Some Considerations Relating to Aero Engine Pyrometry," *AGARD Conference Proceedings No. 399, Advanced Instrumentation for Aeroengine Components*, Philadelphia, PA, Nov. 1986, pp. 17.1–17.14.

[7]Przirembel, H. R., personal communication, Pratt and Whitney Government Engine Business, West Palm Beach, Fl.

[8]Bensing, G. K., personal communication, Rosemount Aerospace Div., Eagan, MN.